

Simulating the summer feeding distribution of Northeast Atlantic mackerel with a mechanistic individual-based model

Article

Accepted Version

Creative Commons: Attribution-Noncommercial-No Derivative Works 4.0

Boyd, R.J., Sibly, R., Hyder, K., Walker, N., Thorpe, R. and Roy, S. (2020) Simulating the summer feeding distribution of Northeast Atlantic mackerel with a mechanistic individual-based model. *Progress in Oceanography*, 183. 102299. ISSN 0079-6611 doi: <https://doi.org/10.1016/j.pocean.2020.102299> Available at <https://centaur.reading.ac.uk/89194/>

It is advisable to refer to the publisher's version if you intend to cite from the work. See [Guidance on citing](#).

To link to this article DOI: <http://dx.doi.org/10.1016/j.pocean.2020.102299>

Publisher: Elsevier

All outputs in CentAUR are protected by Intellectual Property Rights law, including copyright law. Copyright and IPR is retained by the creators or other copyright holders. Terms and conditions for use of this material are defined in the [End User Agreement](#).

www.reading.ac.uk/centaur

CentAUR

Central Archive at the University of Reading

Reading's research outputs online

Simulating the summer feeding distribution of Northeast Atlantic mackerel with a mechanistic individual-based model

Boyd, R.J.^{1,2*}, Sibly, R.³, Hyder, K.^{4,5}, Walker, N.⁴, Thorpe, R.⁴, Roy, S.¹

1) Department of Geography and Environmental Science, University of Reading, Whiteknights, Reading RG6 6AB, UK

2) UK Centre for Ecology and Hydrology, MacLean Building, Benson Lane, Crowmarsh Gifford, Wallingford OX10 8BB, UK

3) School of Biological Sciences, University of Reading, Whiteknights, Reading RG6 6AB, UK

4) Centre for Environment, Fisheries & Aquaculture Science, Lowestoft Laboratory, Pakefield Road, Lowestoft NR330HT, UK

5) School of Environmental Sciences, University of East Anglia, Norwich Research Park, Norwich, Norfolk NR4 7TJ, UK

*Corresponding author; email: robboy@ceh.ac.uk (R. Boyd)

Abstract

Over recent years the summer feeding distribution of Northeast Atlantic mackerel (NEAM, *Scomber scombrus*) has expanded from its traditional core in the Norwegian Sea, northwards towards Svalbard, and westward as far as Greenland. Food availability, temperature and an increase in spawning stock biomass (SSB) are reported to be possible drivers of the distribution, but quantifying the relative contributions of these factors is difficult. Previously we developed a bioenergetics individual-based model (IBM) that uses satellite-derived maps of food availability and temperature to predict NEAM population dynamics. Here, we extend the model to explore the ways in which individuals move in search of food in the summer. We construct models of four possible search mechanisms differing in 1) the extent of the area over which individuals can perceive the environment; and 2) whether or not individuals respond to the local density of conspecifics by avoiding areas in which competition is more intense. We report that the best matches to available data over 2007 to 2015 are obtained when the local density of competitors is taken into account, and individuals move in response to local gradients in feeding opportunities. To determine whether the IBM is able to reproduce the observed north and westward expansion, we record total distribution area, and predicted centre of gravity in terms of latitude and longitude, over 2005 to 2015. The IBM successfully predicts an increase in distribution area, and a northward shift in centre of gravity, over the time series. It also predicts a westward shift in centre of gravity, but to a much lesser extent than has been observed in surveys and the fishery. The inability of our IBM to capture the full extent of the westward expansion suggests that it does not account for all relevant drivers of the NEAM summer distribution. Going forward we hope that our model can be: 1) extended to explore additional drivers of the summer distribution (e.g. currents); and 2) used in a strategic capacity to predict how the NEAM stock may respond to future climate and management scenarios.

Key words

Individual-based model; Atlantic mackerel; geographical distribution; movement mechanisms; bioenergetics; satellite remote-sensing

1. Introduction

Changes in the spatial distribution of fish stocks in relation to jurisdictional boundaries can complicate the division of catch quotas among nations (Fernö et al. 1998, ICES 2016). One recent example is that of Northeast Atlantic mackerel (*Scomber scombrus*, NEAM), a stock with high economic and ecological importance (Trenkel et al. 2014). The majority of the NEAM stock spawns to the west of the British Isles in spring, before migrating northwards to feed in the Nordic seas over summer (Walsh et al. 1995, Uriarte and Lucib 2001). Over recent years the spawning distribution has shifted gradually northwards, likely in response to increasing temperature (Hughes et al. 2014, Bruge et al. 2016). The most extreme change in the NEAM distribution, however, has occurred in the feeding period over summer.

Traditionally, the summer feeding distribution was largely restricted to the Norwegian Sea, but in recent years it has expanded northwards as far as Svalbard, and westwards as far as Greenland (Berge et al. 2015, Jansen et al. 2016). This geographical expansion has resulted in a mismatch between the stock distribution and the historical allocation of catching opportunities, causing 1) political disputes among coastal states in the region (e.g. <https://www.bbc.co.uk/news/uk-scotland-north-east-orkney-shetland-21385888>); and 2) a lack of agreement on overall catch limits such that exploitation has been significantly in excess of scientific advice. Better understanding of the mechanisms driving the NEAM summer expansion would be beneficial from both a scientific and management perspective.

Previous studies have shown that the availability of food is likely a driver of the NEAM summer distribution (Pacariz et al. 2016, Nikolioudakis et al. 2018, Olafsdottir et al. 2018). The geographical expansion coincided with roughly a 100% increase in NEAM spawning stock biomass (SSB) (ICES 2017a), which may have intensified intraspecific competition for the available food in the traditional feeding area. It has been suggested that the resulting food limitation may have provided an incentive for the stock to expand north and westwards in search of better feeding opportunities (Olafsdottir et al. 2018). This hypothesis is supported by a reduction in growth rate over recent years, as reflected in the metrics weight- and length-at-age (Olafsdottir et al. 2016), likely as a result of competition for food among NEAM (Jansen and Burns 2015). Another possibility is that there has been a shift in the locations of the most profitable feeding areas independent of mackerel SSB, i.e. from the bottom-up (Pacariz et al. 2016). In the latter case the shift in the NEAM distribution may simply reflect a similar shift in the distribution of the prey field. The relative contributions of these density dependent and bottom-up drivers to the NEAM geographical expansion are not fully clear.

Recent attempts to investigate the spatial distribution of NEAM have explored the use of correlative species distribution models (SDMs, sometimes called habitat suitability models) (Hughes et al. 2014, Bruge et al. 2016, Nikolioudakis et al. 2018, Olafsdottir et al. 2018). Correlative SDMs are widely-used for establishing relationships between the environment and fish distribution (Robinson et al. 2017), but typically provide limited insight into the underlying mechanisms. It is possible to obtain some mechanistic information using SDMs. For example, Bruge et al. (2016) fitted two separate SDMs to data on NEAM spawning distribution. The first model is based on geographical predictors, and the second is used to determine a thermal niche for spawning activity. By comparing changes in the distribution as predicted by the first model with changes in the location of the thermal niche, the authors were able to show that NEAM spawning activity has shifted northwards at least in part due to ocean warming. There have also been attempts to incorporate mechanisms that underpin species' distributions in SDMs, such as dispersal capacities, i.e. the rates at which animals can move (Holloway et al. 2016), and physiological constraints (Teal et al. 2012, Evans et al. 2015). Despite these advances, however, SDMs are fundamentally correlative and it would

therefore be useful to develop mechanistic models with which hypotheses can be tested about how various drivers affect the distribution of fish stocks.

One mechanistic approach that is becoming increasingly popular as a way to predict fish distribution is with individual-based models (IBMs, also called agent-based models) (e.g. Tu et al. 2012, Utne and Huse 2012, Utne et al. 2012, Watkins and Rose 2017, Heinänen et al. 2018). In IBMs animal populations are represented by their constituent individuals in real-world mapped landscapes (Uchmanski and Grimm 1996, McLane et al. 2011). The individuals each have a unique set of characteristics (e.g. size, location), and the landscapes are characterised by environmental drivers. Detailed models are constructed that describe how the individuals respond to each other and their local environment, and it is from simulation of all the individuals that population measures emerge (van der Vaart et al. 2016). Previously we developed a bioenergetics IBM that predicts NEAM population dynamics based on the rates at which individuals can acquire and use energy from food in the environment (Boyd et al. 2018). This IBM is able to predict temporal variation in population measures (e.g. SSB), but the spatial distribution of the population was largely imposed. For spatial distribution to become an emergent feature of the IBM, algorithms must be incorporated that describe how individuals move in response to their environment (Politikos et al. 2015b, 2015a, Watkins and Rose 2017, Scutt Phillips et al. 2018).

To assess potential mechanisms for the NEAM geographical expansion, we extend our existing IBM (Boyd et al. 2018) to include four alternative models describing how individuals move in search of food during summer. Generally, the profitability of an area in terms of potential feeding opportunities is calculated from sea surface temperature (SST) and surface phytoplankton biomass, both of which are derived from satellite remote-sensing. The movement models represent four search mechanisms which differ in: 1) whether or not the local density of mackerel, and hence competition for food, affects the perceived profitability of an area; and 2) extent of the area over which individuals can detect the environment. Competition for food is central to these movement models, so we start by testing whether or not they can simultaneously fit data on spawning stock biomass (SSB) and weight-at-age. If a model matches these data, we suggest that, at a given stock size, competition for food is realistic as reflected in the individual body weights of the fish. We then use data on the presence/ absence of mackerel in the Nordic seas in July/ August to gauge the relative abilities of each of the four search mechanisms to reproduce the distribution. Finally, we test whether the IBM is able to reproduce the observed north and westward expansion. To do this, we assess how predicted distribution area and the stock's centre of gravity in terms of latitude and longitude change over 2005 to 2015.

2. Methods

2.1. Model overview

In this section we first give a brief overview of the previous IBM (Boyd et al. 2018) on which we build here, followed by the additions made for this paper. For the IBM's full technical specification see the "TRANSPARENT and Comprehensive model Evaluation" (TRACE) document in the supplementary material. In section 2 of the TRACE we provide a full model description in the standard Overview Design concepts and Details (ODD) format (Grimm et al. 2006).

In broad terms, the model landscape consists of dynamic maps of sea surface temperature SST and surface phytoplankton density, which we use to represent baseline food availability (Fig. 1). Both variables are derived from satellite remote-sensing. The modelled fish population represents the western spawning component of the North East Atlantic mackerel

stock as defined by the International Council for the Exploration of the Seas (ICES). It should be noted that, while ICES treat NEAM as comprising isolated spawning units, there is evidence of straying between the western and North Sea spawning components (Jansen and Gislason 2013). Before its collapse in the 1970s the North Sea component was substantial (Jansen 2014). However, over the time period considered in this study, there has been limited spawning in the North Sea (typically < 5% of spawners) whereas the western component has remained stable at around 80% of the stock's total biomass (ICES 2014a, 2014b, 2017b). Fish are grouped into super-individuals (SI), which comprise a number of individuals with identical variables (Scheffer et al. 1995). SIs move around the landscape according to their life cycles (e.g. to spawn, feed and overwinter). Each SI has an energy budget which determines how its characteristics (e.g. body size, life stage, energy reserves) change in response to local food availability and SST. Time- and age-varying fishing pressure determines the rate of mortality from exploitation. Each year a constant number (n_{cohort}) of SIs are introduced as eggs at spawning time, but the abundance that they represent is determined by the amount of energy the spawning stock has put into egg production. The amount of energy that can be allocated to egg production is an emergent feature of the energy budget and reflects the feeding opportunities available to adults prior to spawning. Abundance reduces as mortality is applied throughout life. Population measures such as SSB and recruitment are obtained by summarising the characteristics of all the SIs including their abundances.

In this paper we focus on the adult feeding period, specifically July and August, so as to match the available data. After spawning, adults enter the feeding area and begin to actively seek out the most profitable locations. Profitability is defined as potential ingestion rate in that area, based on food availability and SST. We further divide this into two assumptions about what defines a profitable area: one including an effect of competition for food among the mackerel; and a second that is independent of mackerel density (see section 2.3.3). The ways in which SIs are directed towards the most profitable areas are modelled with one of a gradient area search (GAS) or ideal free distribution (IFD) feeding strategy (see section 2.3.4), which contain different assumptions about how much environmental information they have access to. We combine the assumptions about feeding strategy and density dependence to generate four possible search mechanisms: a density-dependent (includes competition for food) gradient area search (GAS_{dd}); a density-independent (does not include competition for food) gradient area search (GAS_{di}); a density-dependent ideal free distribution (IFD_{dd}); and a density-independent ideal free distribution (IFD_{di}). See Table 1 for a summary of the characteristics of each search mechanism and section 2.3 for full details. We then test which model best matches various mackerel population data.

Table 1. Summary of the characteristics of each search mechanism (movement model). Competition effect indicates whether or not individuals take conspecific density into account when assessing a patch's profitability. Temporal resolution is the frequency at which individuals' positions are updated. Environmental information accessible indicates the extent of the area over which individuals can detect the environment. Space indicates whether the model works in the continuous or discrete (patch by patch) space of the model grid.

Search mechanism	Competition effect?	Temporal resolution	Environmental information accessible	Space
IFD_{dd}	Yes	Five-day	Area reachable in five days	Discrete

IFD_{di}	No	Five-day	Area reachable in five days	Discrete
GAS_{dd}	Yes	One-day	Neighbouring cells	Continuous
GAS_{di}	No	One-day	Neighbouring cells	Continuous

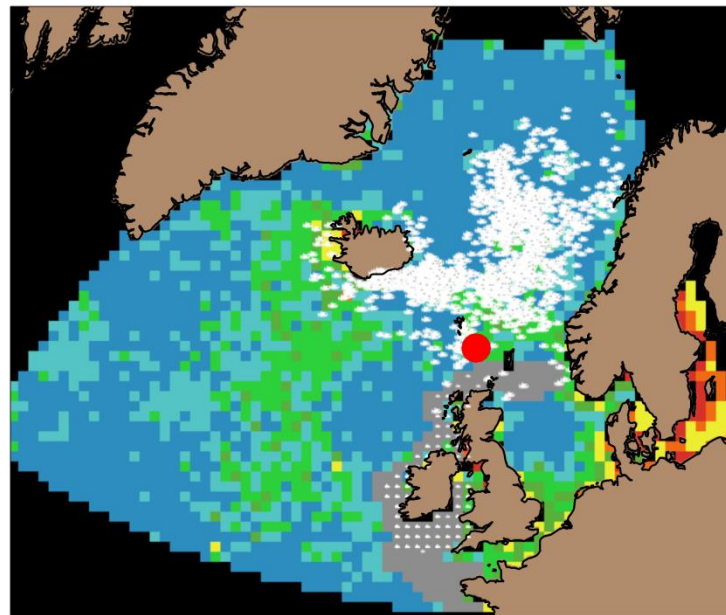


Figure 1. Snapshot of the IBM interface on August 1st 2011. Grey patches denote the shelf edge (cells to the North and West of the British Isles on which $50\text{m} < \text{depth} < 550\text{m}$ and $\text{latitude} < 60.5^\circ\text{N}$). The red point shows the entrance to the feeding area in the Norwegian Sea (61.5°N , -4.8°W). Large white fish in the Nordic sea are adults, and the smaller fish to the west of the British Isles are juveniles. The colour of the landscape corresponds to phytoplankton density: blue represents low density, then green, yellow and red which indicates high density. The colour bins are arbitrary.

2.2.State variables and scales

The model landscape comprises a two-dimensional grid of patches of sea surface (Fig. 1). The spatial extent spans from 47 to 77°N , and from -45° to 20°E . Each patch represents $60 \times 60 \text{ km}$ (Lambert Azimuthal equal area projection) and is characterised by food density, sea surface temperature (SST) and mackerel density (g patch^{-1}), from which profitability indices

are calculated (section 2.3.3). The mackerel population is represented by a constant 4000 SIs; as n_{cohort} new SIs enter the model at spawning time each year an equal number reach terminal age (>15 years) and are removed from the model. Each SI is characterised by age, gender, life stage (egg, yolk-sac larvae, larvae, juvenile or adult), length, mass (structural, lipid and gonad), abundance and location (see TRACE section 2 for details of initialisation). The temporal extent spans from January 1st 2005 to December 31st 2015. The model proceeds in discrete five-day time-steps.

2.3. Model description

For the purposes of this study, key aspects of the model are: 1) the bioenergetics; 2) the migrations of adult mackerel into and out of the feeding area; 3) the cues used to determine how profitable each patch is; 4) the feeding strategies used to direct adults to the most profitable patches; and 5) the coupling of the movement and the bioenergetics. See TRACE section 2 for a full description of the IBM including the bioenergetics and the pre-adult phases of the life cycle.

2.3.1. Bioenergetics

Individuals obtain energy from phytoplankton which is used as a proxy for prey availability. Size-based cannibalism is possible in the IBM, but adults do not overlap with sufficiently small individuals over summer so it is not relevant here. Ingestion rate is a function of food density, body surface area, SST and local mackerel density. A proportion of the energy ingested from food is assimilated and made available to the vital processes maintenance (metabolic rate), growth, reproduction and energy storage. The rates at which energy is allocated to these processes depend on temperature and body size. The effect of temperature on energy acquisition and expenditure is generally given relative to a reference temperature T_{ref} using an exponential Arrhenius function $A(\text{SST})$, as:

$$A(\text{SST}) = e^{\frac{-E_a}{K} \left(\left(\frac{1}{\text{SST}} \right) - \left(\frac{1}{T_{\text{ref}}} \right) \right)} \quad (1)$$

where E_a is the activation energy, K is Boltzmann's constant (see TRACE section 2 for a full list of parameters and section 7 for a local sensitivity analysis). The partitioning of energy to vital processes depends on an individual's life stage and time of year. See Sibly et al. (2013) for an overview, and TRACE section 2 for full details.

2.3.2. Migrations in to and out of the feeding area

The feeding migration of mackerel into the Norwegian Sea coincides with spawning, and occurs primarily along the European shelf edge to the west of the British Isles (Brunel et al. 2017). We represent the shelf edge with a corridor around the British Isles in which $-550\text{m} < \text{depth} < -50\text{m}$ and $\text{latitude} < 60.5^\circ \text{ N}$ (Fig. 1). Each patch on the shelf edge is characterised by its distance D (patches) from the target destination at the entrance to the Norwegian Sea ($61.5^\circ \text{N } 4.8^\circ \text{W}$, red circle in Fig. 1). After spawning (see TRACE section 2 for details), SIs move north and east along the shelf edge to the patch with the lowest D within their possible swimming range. An individual's possible swimming range is calculated from its minimum swimming velocity V_{min} (km hr^{-1}), given as a function of standard body length L_s and the caudal fin aspect ratio A_r (Sambilay Jr 1990):

$$V_{\text{min}} = V_0 L_s^{a_v} A_r^{b_v} \quad (2)$$

where V_0 is a normalizing constant, and a_v and b_v are scaling exponents. Velocities are converted to distance using the appropriate time period, here one time-step of five days. This algorithm fulfils the needs to: 1) direct SIs from the spawning to feeding areas north and

eastward along the shelf edge; and 2) for migration rate to increase with body length (Jansen and Gislason 2011). To prevent all individuals congregating at the same destination patch as they enter the Norwegian Sea, each individual is forced to stop migrating at a randomly-selected distance from the destination in which $D < 5$ patches (at this point one of the four search mechanisms in Table 1 start to direct movement). The return overwintering migration is simply the reverse of the feeding migration (back towards the entrance to the Norwegian Sea) and begins on October 1st (see TRACE section 2 for details).

2.3.3. Profitability cues

After reaching their destination in the feeding area, SIs begin to seek out the most profitable patches on which to feed. The profitability of a patch is defined using one of two cues, each representing possible ingestion rate with a different assumption about density dependence. The first cue c_{di} represents the bottom-up effect of phytoplankton density as a proxy for food availability, and the effect of SST (Kelvins), in the form of a Holling type 2 functional response:

$$c_{di} = A(SST) \frac{X}{X + h} \quad (3)$$

where X is phytoplankton density (g m^{-2}) and h is a half saturation constant and $A(SST)$ is an Arrhenius function (eq. 1). The second cue c_{dd} is similar to c_{di} but also includes a density-dependent effect of competition for food among the mackerel, according to a Beddington-DeAngelis functional response:

$$c_{dd} = A(SST) \frac{X}{X + h + cD} \quad (4)$$

where D is mackerel density and c determines the strength of the density dependence. It is important to note that although c_{di} does not include an effect of mackerel density, an individual's ingestion rate is always affected by the competition term, cD , in eq. 4.

Studies using sonar have shown that the prevailing swimming direction of NEAM in summer is northwards (Nottestad et al. 2016). One possible explanation for this is photoperiod; mackerel are visual feeders (Pepin et al. 1988) so moving to higher latitudes in summer would permit extended feeding periods, which is not captured by equations 3 and 4. To reflect this, we up-weight the values of c_{di} and c_{dd} on patches north of an individual's current position by a factor $\text{photo}_{\text{effect}}$ (i.e. we include an implicit effect of photoperiod on patch profitability). For each search mechanism we test three values of $\text{photo}_{\text{effect}}$: 1 (i.e. no effect of photoperiod), 1.25 and 1.5. We adopt the value for each search mechanism that maximises its ability to match the occurrence data in Fig. 4. See TRACE section 7 for full details and for the sensitivities of predicted distribution to $\text{photo}_{\text{effect}}$.

2.3.4. Feeding strategies

The ways in which SIs seek out the most profitable feeding patches are modelled with one of an ideal free distribution (IFD) or gradient area search (GAS) feeding strategy, outlined below.

Ideal free distribution: in the IFD feeding strategy we assume that SIs can detect the environment in all patches within their five-day search area. This implies the use of predictive orientation, i.e. where individuals orientate towards areas that are predicted to be optimal, without necessarily using information in the near-field (Fernö et al. 1998). A five-

day search area was chosen to match the model time-step. The radius of an individual's search area is calculated from its realised swimming velocity V_r , given as $V_r = V_{\min} + (V_{\min} \epsilon)$, where ϵ is drawn randomly from a uniform distribution over the range 0 to 1, and V_{\min} is minimum swimming velocity (eq. 2). This algorithm produces realised swimming velocities in the range 1.85 to 4.42 km hour⁻¹ (assuming body lengths in the range 30 to 40 cm). This is similar to swimming speeds observed in the Norwegian Sea over summer using sonar. Godø et al. (2004) observed the majority of NEAM schools to be swimming between 0 and 3.6 km hour⁻¹, but with many swimming considerably faster. In a laboratory setting a maximum sustained speed of 4.41 km hour⁻¹ was observed for a 35 cm fish (He and Wardle 1988, cited by Walsh et al. 1995). The IFD sub-model works in discrete space on a patch by patch basis: SIs simply move each time-step to the most profitable patch within their search area and on which SST \geq the lower boundary (7° C) below which mackerel avoid (Olafsdottir et al. 2018).

Gradient area search: the GAS feeding strategy is broadly similar to that presented by Politikos et al. (2015) and Tu et al. (2012). It differs from the IFD in three keys ways: 1) SIs can detect the profitability of the four neighbouring patches in x and y dimensions only, meaning they have access to considerably less environmental information than in the IFD; 2) the GAS model works in the continuous space of the model grid; and 3) SI's locations are updated more frequently at five times per time-step (i.e. once per day), to ensure that they cannot overshoot the neighbouring patch. Positions in x and y dimensions are updated by:

$$\begin{aligned} x_{t+1} &= x_t + (D_x + R_x) \\ y_{t+1} &= y_t + (D_y + R_y) \end{aligned} \quad (5)$$

where D_x and D_y are the directed search part of the equation, and R_x and R_y are the random components.

In the orientated part of eq. (5) D_x , D_y , SIs compare the profitability at their current location with that of the day before. If it has become more profitable, they will continue to swim in the same direction as the oriented part of their movement the day before. If a SI's current environment is less profitable than the day before, they follow a gradient search towards what is perceived to be the most profitable patch based on information in x and y dimensions, at velocity V_r (see ideal free distribution in section 2.3.4), given by:

$$\begin{aligned} D_x &= V_r \frac{c_x}{\sqrt{c_x^2 + c_y^2}} \\ D_y &= V_r \frac{c_y}{\sqrt{c_x^2 + c_y^2}} \end{aligned} \quad (6)$$

where c_x and c_y are the gradients of the profitability cues (eq. 3, 4) in x and y dimensions. This amounts to what is called a state-location orientation mechanism (basing new orientation on a comparison of the current and previous environment), and there is some indication that herring follow a similar strategy in the Norwegian sea (Fernö et al. 1998). Following Politikos et al. (2015a) we assume that movement is directed (D_x , D_y) for 12 hours day⁻¹, and movement in the other 12 hours follows the random component of eq. 5 R_x , R_y , which we give as swimming at velocity V_{\min} in a random direction. This assumption introduces

stochasticity into the GAS models and prevents unrealistic overcrowding on optimal patches (particularly in the GAS_{di} model in which competition is not accounted for).

As with the IFD, we prevent SIs from moving into patches with intolerably low temperature. In the oriented part of eq. 5, we repel individuals from patches with SST < 7°C by setting profitability cues in those areas to 0. For the random component of eq. 5, if a SI's orientation would direct it on to a patch with SST < 7°C, its heading is reversed.

2.3.5. Movement-bioenergetics coupling

The energy cost of searching for food is subsumed into an individual's active metabolic rate AMR. AMR is given as a function of SST, body mass M and swimming velocity V as:

$$AMR = a_{AMR} M^{b_{AMR}} V^{c_{AMR}} A(SST) \quad (7)$$

where a_{AMR} is a normalizing constant, b_{AMR} and c_{AMR} are scaling exponents, and V is given by $V = (V_r + V_{min}) / 2$, i.e. assuming that half of each day is spent at V_{min} , and half at V_r .

2.4. Model simulations

The model simulates the full life cycle of the mackerel population from January 1st 2005 to December 31st 2015. In this paper we focus on the summer feeding period in each year, and model the ways in which individual adults move in search of the best feeding opportunities. This is represented by one of four search mechanisms spanning each combination of profitability cue and feeding strategy (e.g. IFD_{dd}, IFD_{di}, GAS_{dd}, GAS_{di}). Simulations are forced by fishing mortality F at age, phytoplankton density X and SST. F is updated every year. Maps of X and SST represent ten-day composites and are updated accordingly.

For the purposes of this paper, outputs that are recorded annually include: SSB at spawning time (May 1st), mean weight-at-age in summer (August 1st), whether or not mackerel were present on each patch in July or August, and mean mackerel density on each patch over July/August. From these measures we calculate total summer distribution area as the sum of the areas of patches on which mackerel was present, and the centre of gravity of the stock in terms of latitude (COG_y) and longitude (COG_x). As we have changed our IBM structurally since Boyd et al. (2018), we provide updated model fits to separate data on various aspects of the population structure in TRACE section 9. The times at which outputs are recorded were chosen to match the available data as closely as possible.

2.5. Data

Input data includes F (day⁻¹), and maps of phytoplankton density X (g m⁻²) and SST (kelvins). F comes from the stock assessment as age-specific rates that vary annually, and are applied each day to the appropriate age group. X and SST were derived from data from the MODIS sensor on NASA's Aqua satellite (NASA OBPG 2017a, 2017b). Ten-day composites are used at a spatial resolution of 60 x 60 km. The satellite remote-sensing data required processing for use as model input (e.g. re-gridding and interpolations), the details of which can be found in TRACE section 3.

The model was calibrated with estimates of SSB (spawning time) from the 2017 NEA mackerel stock assessment, and mean weight-at-ages 3 and 13 in the summers of 2007 and 2010-2015 from the International ecosystem survey in the Nordic Seas (IESSNS) (see Nøttestad et al (2015) for full details of the data). We scale the SSB data by a factor of 0.8 to reflect the fact that we only represent the stock's western spawning component which

comprises ~ 80% of its total biomass. We calibrated the IBM with data on SSB and weight-at-age because its ability to fit them simultaneously would indicate that competition for food at a given stock size is realistic as reflected in the body weights of the fish. This is important because density dependence is a key feature of the movement sub-models. Full details of the data are provided in TRACE section 3.

To validate the model we used data from the IESSNS on the presence/ absence of mackerel in the Nordic seas in July/ August of 2007 and 2010 to 2015 (see Nøttestad et al. (2015) for details). We approximated these data from Fig. 2 of Olafsdottir et al. (2018) using Java's PlotDigitizer (<http://plotdigitizer.sourceforge.net/>).

2.6. Model calibration

For each search mechanism (IFD_{dd} etc.) we calibrated three parameters: background early mortality M_e (natural mortality rate for eggs and larvae excluding explicit cannibalism in the IBM), strength of the density dependence (c) and the half saturation constant (h). We estimated the parameters by fitting the model to the calibration data (see data) using rejection approximate Bayesian computation (ABC) (van der Vaart et al. 2015). In broad terms, we ran 1000 simulations for each search mechanism, while randomly sampling values of the three parameters from uniform prior distributions. We then “accepted” the parameters that minimised the sum of the squared deviations of the model outputs from the data. See TRACE section 3 for full details.

2.7. Search mechanism model selection

To determine which search mechanism was best able to reproduce the mackerel summer distribution, we compared their predictions of presence/ absence to the data in Fig. 4. First, we assessed the fits of each model by testing for an association between their predictions and the data with a chi square test. We then further quantified the performance of each sub-model using standard statistics for binary data: sensitivity, i.e. the proportion of observed presences correctly classified; specificity, i.e. the proportion of observed absences correctly classified; and the distance to the top left corner on a plot of sensitivity as a function of $1 - \text{specificity}$ (Fig. 5), $d(0, 1)$, chosen because this point (0, 1) corresponds to a perfectly classified model (sensitivity and specificity of 1) (Cantor et al. 1999, Liu et al. 2005). We include the measure $d(0, 1)$ instead of, for example, an overall accuracy rate, because it is robust to disparity in the prevalence of presences and absences which is high in these data (~82% presences). When comparing predictions of a continuous distribution (here density) to data on presence/ absence it is useful to determine a threshold representing the minimum density that should be considered a presence, with everything below this density being classified as an absence. We optimised a threshold density for each search mechanism using the measure $d(0,1)$ as a cost function (Cantor et al. 1999, Liu et al. 2005). See TRACE section 7 for full details and presence thresholds. By pooling the data for all years in our analysis we give extra weight to years with greater sampling effort, which we consider appropriate.

2.8. Change in predicted distribution over 2005 to 2015

To test whether our IBM can reproduce the observed north and westward expansion of NEAM over summer, we record total distribution area, COG_x ($^\circ$ W) and COG_y ($^\circ$ N) over July/ August of 2005 to 2015. We regress each summary statistic on simulation year and if the slopes are positive significant, then we consider the search mechanism able to reproduce the expansion.

3. Results

3.1. Model calibration

In order to test each model's ability to represent the effects of competition for food, we fitted them to available data on SSB and weight-at-ages 3-13 over 2005 to 2015 (Figs. 2, 3; see TRACE section 3 for estimated parameter values). We suggest that if a sub-model can simultaneously match these data, then competition for food at a given SSB is sufficiently realistic. SSB generally shows an increasing trend over the calibration period (Fig. 2), so we also present model predictions in 2016 and 2017 to show that the IBM predictions do not simply continue to rise. To quantify the goodness of fits to the data (including 2016 and 2017), we used three commonly-used diagnostics for each variable: the correlation coefficient r ; the root mean square error (RMSE); and the bias (Edwards et al. 2012, Formenti et al. 2015). Overall we suggest that each model can fit data on both SSB and weight-at-age reasonably well. The search mechanisms produce similar trajectories for SSB. From 2011 the IFD_{dd} model diverges slightly from the other models because individuals have better feeding opportunities which is reflected in higher SSB. SSB is generally matched well, with r being ≥ 0.84 ($p < 0.0003$) and $RMSE < 0.51$ million tonnes in all cases (Table 1). For weight-at-age the correlations are lower than for SSB (0.36 to 0.50), but the overall biases are small at ≤ 10.81 g (Table 1). With all search mechanisms the IBM is able to capture the general downward trend in weight-at-age (Fig. 3). However, for ages seven and below, the IFD models are unable to predict the increase in weight-at-age observed near the end of the time series.

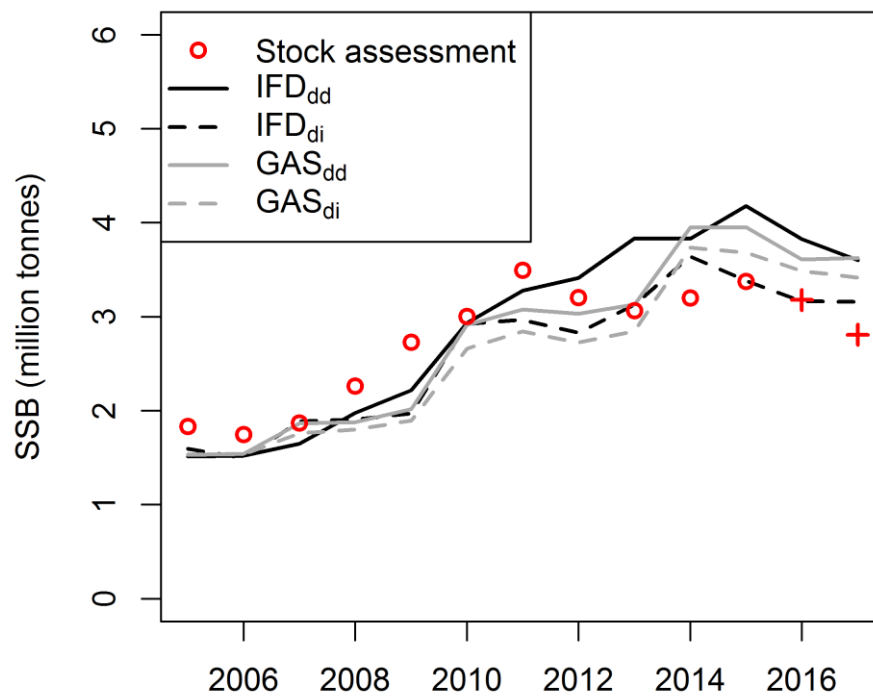


Figure 2. Predicted SSB from each feeding sub-model compared with estimates from the stock assessment. Values represent means over ten simulations. Note that the IBM was fitted to the data over the period 2005 to 2015 (red circles) and not to the data in 2016 or 2017 (red crosses).

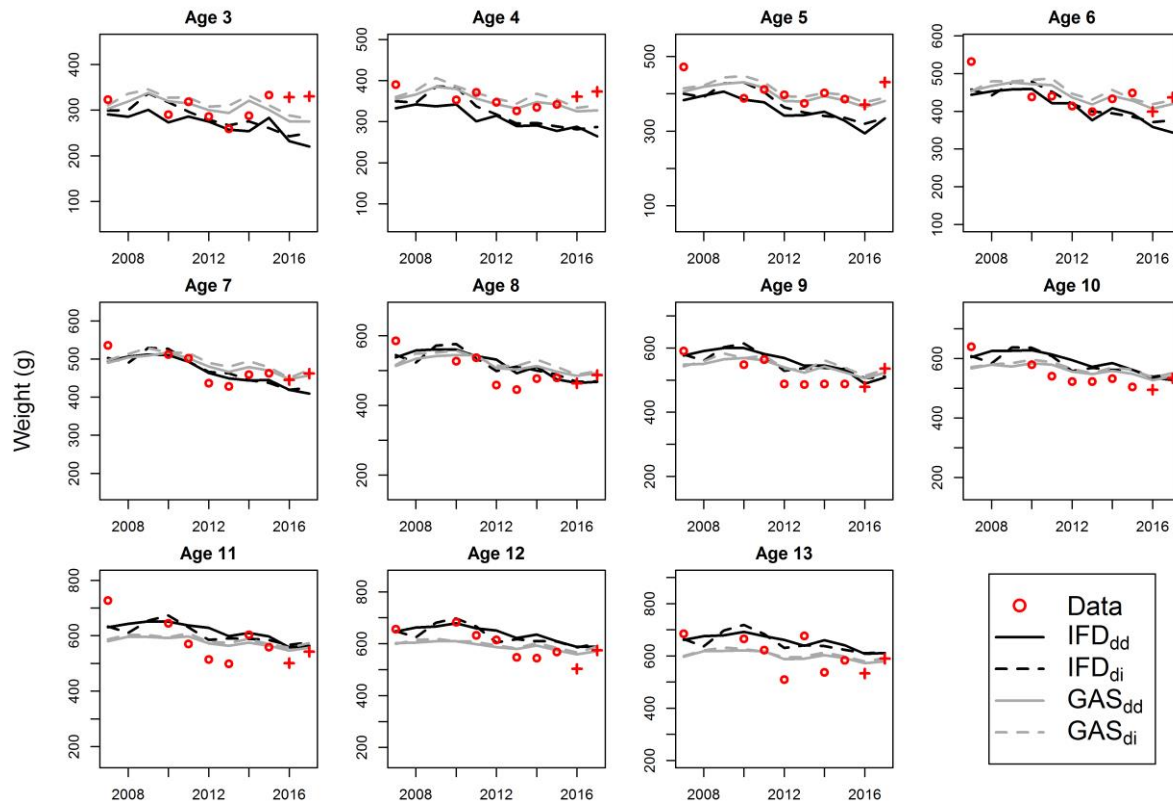


Figure 3. Predicted mean weight-at-ages 3-13 in summer from each feeding sub-model compared with data from the International Ecosystem Survey in the Nordic Seas (IESSNS). Values represent means over five simulations. Note that the model was fitted the data over 2007 to 2015, and not to the data in 2016 or 2017 (red crosses).

Table 1. The goodness of fit between predicted and observed SSB and weight-at-age for each sub-model. For weight at age we present the mean r over all age groups, and RMSE and bias are aggregated over all age groups. All diagnostics are based on means over ten simulations. Units are in millions of tonnes for SSB, and grams for weight-at-age.

Model	SSB			Weight-at-age		
	r	RMSE	Bias	Mean r	RMSE	Bias
GAS_{dd}	0.87	0.46	-0.03	0.46	40.32	-1.75
GAS_{di}	0.84	0.46	0.14	0.36	43.48	-10.81
IFD_{dd}	0.91	0.51	-0.15	0.50	55.30	-0.67
IFD_{di}	0.89	0.35	0.13	0.54	48.57	-4.70

3.2. Search mechanism model selection

To determine which search mechanism is best able to reproduce the NEAM summer distribution we compared their predictions to data on presence/ absence in the Nordic Seas. A

threshold was optimised for each search mechanism representing the minimum density that should be classed as a presence (see TRACE section 7). Predictions obtained from all search mechanisms are all significantly related to the data (Chi square, $p < 0.01$). The GAS models produce similar results in terms of sensitivity, specificity and hence $d(0,1)$ (Table 2, Fig. 5). The IFD models, on the hand, produce very different results. The IFD_{dd} shows reasonably good sensitivity and specificity (0.61 and 0.67, respectively). The IFD_{di} search mechanism has a high specificity, but a very low sensitivity (discussed in section 4). The measure $d(0,1)$ suggests that the GAS models, in particular the GAS_{dd}, are best able to reproduce the NEAM summer distribution and should be used in future work.

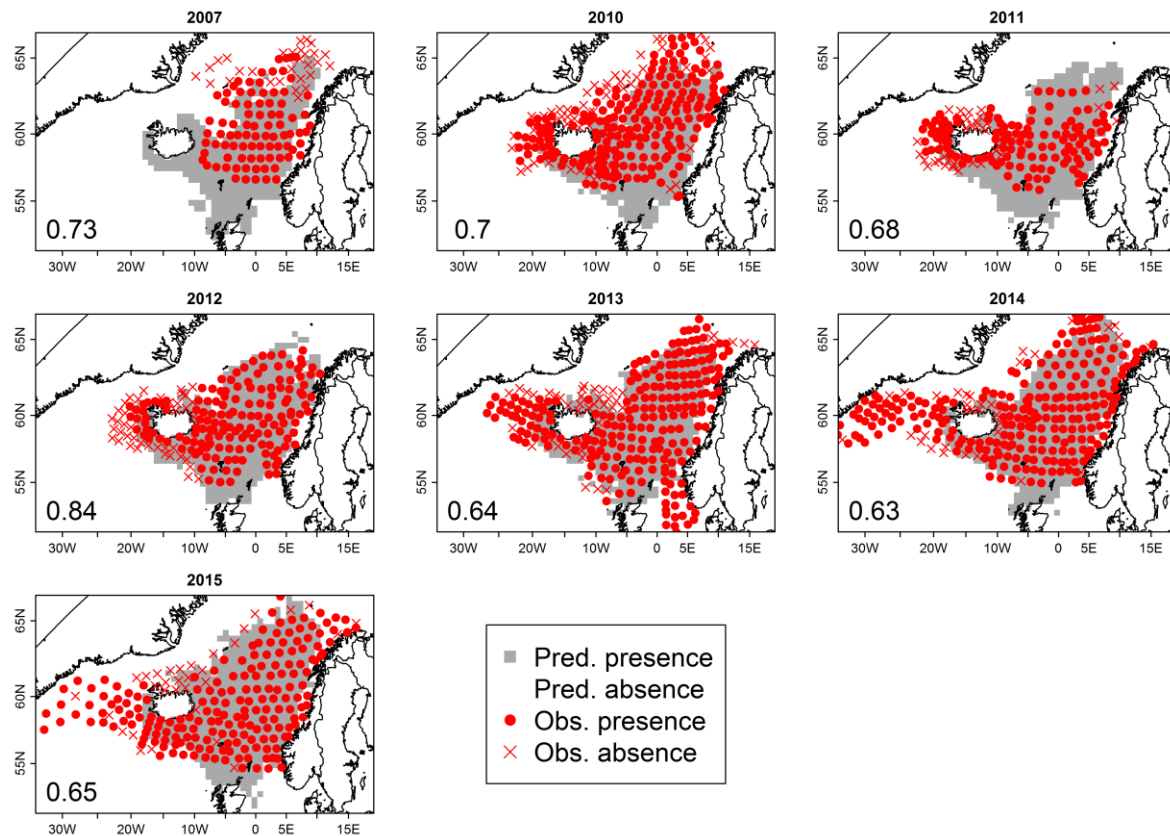


Figure 4. Data from the IESSNS survey (approximated from Olafsdottir et al. (2018)) on presence (obs. presence) and absence (obs. absence) of mackerel in the Nordic seas over July/August. We also show simulated presence (pred. presence) and absence (pred. absence) as predicted by the GAS_{dd} search mechanism. It should be noted that predicted presence is obtained after optimising a threshold density below which an area is classed as an absence. This means that the areas of low density on the fringes of the distribution (e.g. in the western area) are not shown as presences here. The numbers on each panel indicate the proportion of data points in each year for which the model correctly predicted whether or not mackerel was present.

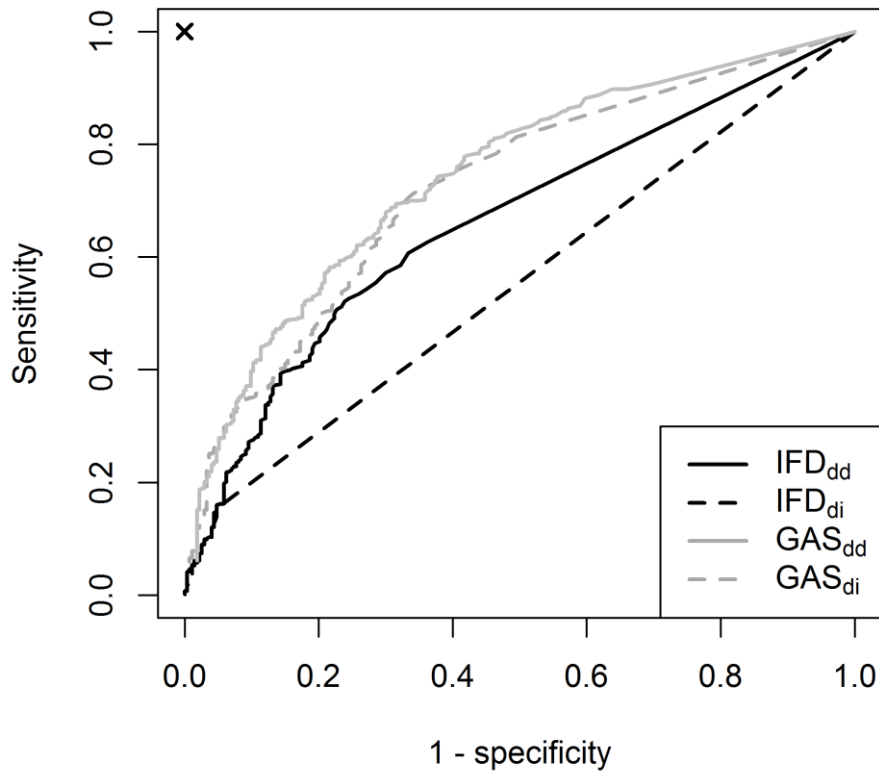


Figure 5. Sensitivity plotted against 1- specificity (loss of specificity) for each search mechanism's predictions of mackerel presence/ absence in July/ August. Curves represent varying density thresholds (above which an area is classed as a presence) over the range 0 to 30% of maximum predicted density in each search mechanism. A model at point 0, 1 (black cross) would have perfect sensitivity and specificity. Values are derived from means over 10 simulations.

Table 2. Statistics indicating the ability of each sub-model to reproduce the data on presence/ absence of mackerel in Fig. 4. $d(0,1)$ is the distance of each model to point 0,1 (corresponding to a perfectly sensitive and specific model) on Fig. 5. Better models achieve lower values of $d(0,1)$. Values are derived from means over ten simulations after optimising the threshold density for what defines a presence.

Model	Sensitivity	Specificity	$d(0,1)$
GAS_{dd}	0.69	0.70	0.44
GAS_{di}	0.67	0.70	0.45
IFD_{dd}	0.61	0.67	0.52
IFD_{di}	0.15	0.95	0.85

3.3. Predicted expansion

To test how predicted mackerel summer distribution changes through time, we recorded three summary statistics in each year: total distribution area, COG_x , and COG_y . For these simulations we used the best-performing GAS_{dd} search mechanism (Fig. 5), but also the

IFD_{dd} as inspection of the outputs suggested that the latter was better able to capture the western extent of the distribution (the IFD_{di} and GAS_{di} models were not). For both search mechanisms we regressed distribution area, COG_x and COG_y on simulation year, and all of the slopes were positive and significant ($p < 0.05$). This shows that the models are in agreement with the general consensus that the stock's distribution area increases through time, and that its centre of gravity shifts north and westwards (Fig. 6).

To explore possible differences in the distribution changes predicted by the GAS_{dd} and IFD_{dd} search mechanisms, we compared their predictions of distribution area, COG_x and COG_y. For each summary statistic, the rates of change are similar between search mechanisms (Fig. 6). This is indicated by a lack of interaction effects between search mechanism and simulation year (i.e. the slopes are not significantly different; ANCOVA, $p > 0.05$). There is an effect of search mechanism on COG_y ($p < 0.05$) which indicates that, although the slopes are similar, there is a significant difference in y intercepts between models (Fig. 6c). This can be explained by the fact that, while the cores of the distributions predicted by the two models are similar (Norwegian Sea and around Iceland; Figs 7 and 8), the GAS_{dd} model generally predicts a more northerly distribution than the IFD_{dd}. It should be noted that an increase in distribution area with stock size is expected due the competition term, cD, in equation 4.

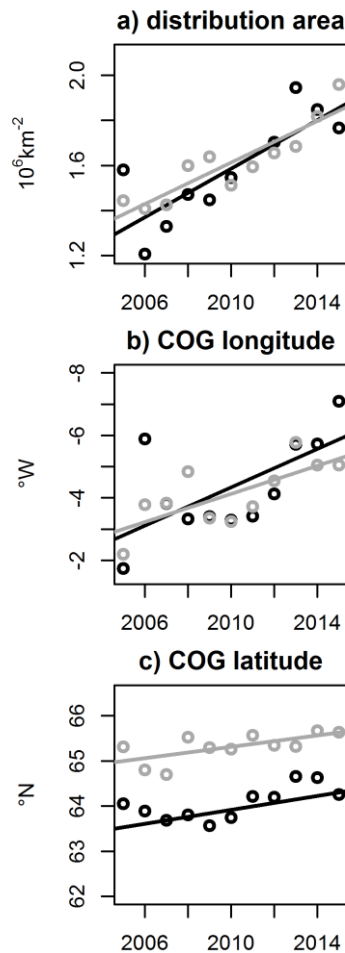


Figure 6. Comparisons of a) distribution area, b) centre of gravity in terms of longitude COG_x and c) centre of gravity in terms of latitude COG_y as predicted by the GAS_{dd} (grey circles) and IFD_{dd} (black circles) search mechanisms.

NEAM density in in July/ August of each year is presented for the GAS_{dd} and IFD_{dd} search mechanisms in figs 7 and 8, respectively. Generally the models agree on the areas of highest

density such as the Norwegian Sea and around Iceland. The models also both produce a similar boundary at the northern limit of the distribution around the position of the 7° C isotherm (north of which mackerel avoid). This boundary is particularly evident to the northwest of Iceland where the cool East Greenland Current flows south. The key differences between the models are that the IFD_{dd} produces a patchier distribution, but is better able to capture the western extent of the distribution as observed in the IESSNS (e.g. high densities west of Iceland; fig. 4; discussed in section 4).

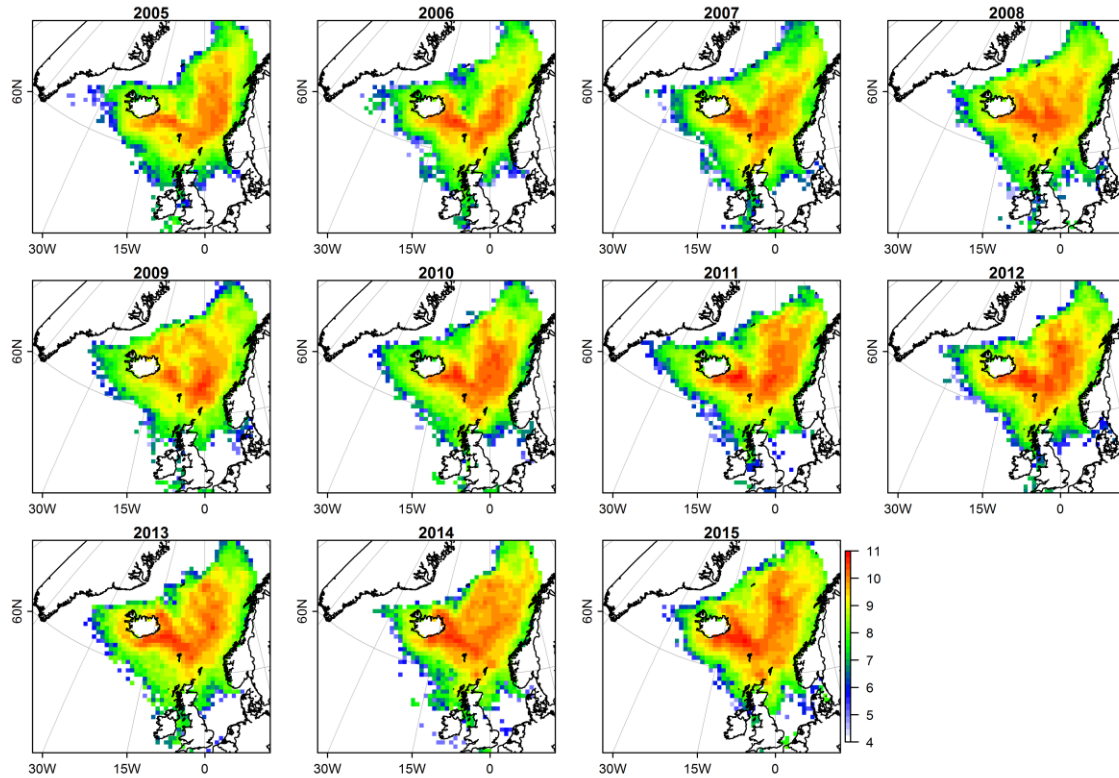


Figure 7. Mackerel density (g patch⁻¹) in the summer of each year on a log10 scale as predicted by the GAS_{dd} search mechanism. Values represent means over July/ August, and over ten simulations. Note that predictions here do not correspond exactly to those in fig. 4 where areas of low density (e.g. the fringes of the distribution here) are classed as absences.

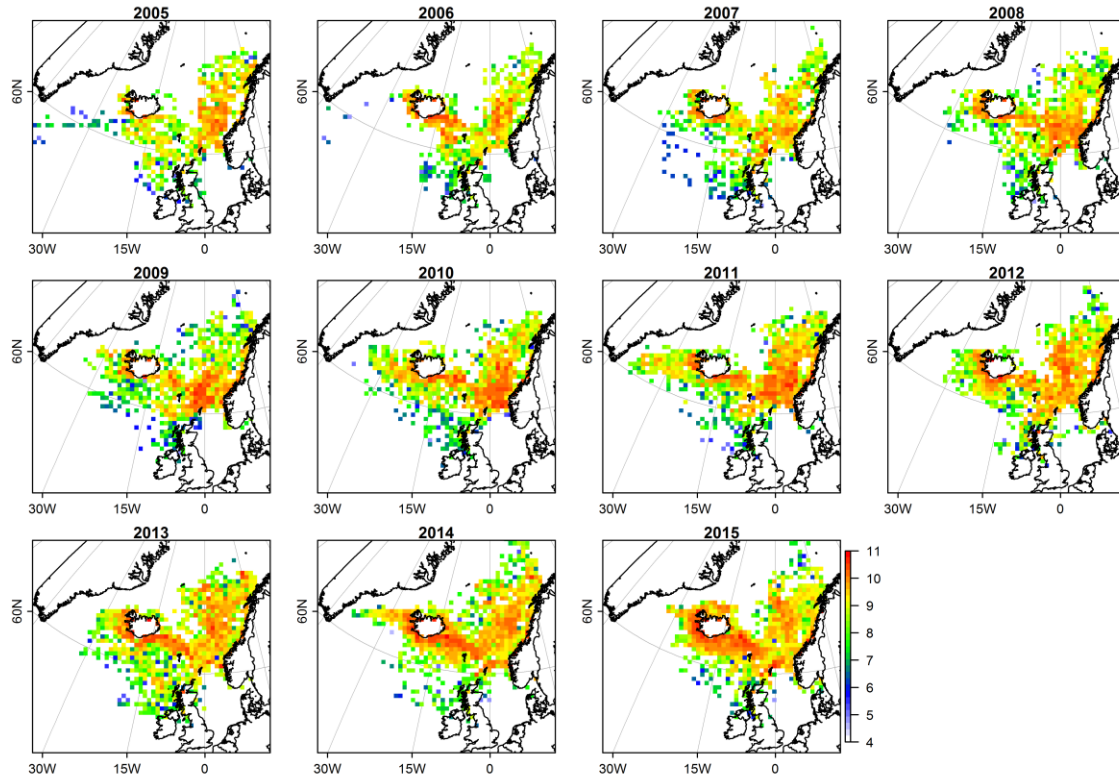


Figure 8. Mackerel density (g patch^{-1}) in the summer of each year on a log10 scale as predicted by the IFD_{dd} search mechanism. Values represent means over July/ August, and over ten simulations.

4. Discussion

We have coupled an existing bioenergetics IBM to models describing how mackerel move in search of food during summer. The models contain alternative assumptions about: 1) whether or not mackerel density, and hence competition for food, affect the perceived profitability of an area; and 2) the extent of the area over which individuals can detect the environment. After comparing the outputs of each sub-model to data on SSB, weight-at-age and mackerel occurrence, we suggest that a gradient area search feeding strategy, in which competition for food affects the perceived profitability of an area, and SIs can detect the environment in the near field only, performs best. We then tested whether or not the IBM is able to reproduce the observed north and westward expansion. With the best-performing search mechanism the IBM is able to reproduce the change in distribution, as indicated by an increase in distribution area and a north and westward shift in centre of gravity. However, the IBM is not able to capture the full extent of the expansion in the western direction.

Selecting the best search mechanism based on the occurrence data was not straightforward. Initially we looked at the sensitivities and specificities of each search mechanism while assuming that patches with mean density > 0 represent a presence. The GAS models performed poorly under this assumption because, due to inclusion of stochastic movements, they predict that a small number of individuals end up on sub-optimal patches. This was reflected by high “false positive” rates and specificities of $< 40\%$. However, when the threshold defining the minimum density that constitutes a presence is optimised, the GAS feeding strategy performs best. This is because patches with very low density (but > 0) no longer count as presences hence the false positive rates of the GAS models are reduced.

Once the density thresholds are optimised we suggest that the GAS models are best and should be used in future work.

In Table 2 it can be seen that the GAS models perform similarly in terms of sensitivity and specificity, but the IFD models are very different. This reflects the different assumptions made in the feeding strategies. In the GAS models individuals can only detect the environment in neighbouring patches, and there is a stochastic component to their movement. As such under this feeding strategy individuals are less likely to locate optimal patches, and if they do it is possible that the random movement will displace them. On the other hand, in the IFD feeding strategy individuals can detect the environment over a much larger area, and there is less stochasticity in their movements. As a result, individuals are more likely to locate and move to optimal patches and are less likely to leave. This means that density dependence becomes very important in the IFD search mechanism. In the IFD_{dd} patches become increasingly unattractive as mackerel density increases, causing individuals to spread out. In the IFD_{di}, however, individuals do not account for local mackerel density; they congregate on patches with high phytoplankton density and of suitable temperature regardless of competition for the food. This is reflected in a very patch distribution, high “miss rates” and hence low specificity.

The relative abilities of the GAS and IFD search mechanisms to match data on NEAM presence/ absence give insight into the possible ways in which mackerel seek out the best feeding opportunities. In the GAS search mechanism, the directed search component of movement is based solely on a reactive mechanism, i.e. a near-field response to gradients in the profitability cues. In this feeding strategy, individuals are directed to locally-optimal areas, but often do not reach the most profitable areas which can be further afield (e.g. in the western expansion area). On the other hand, in our IFD sub-model individuals can access information about the environment over a much larger area, and, at least in the IFD_{dd} formulation, tend to reach more profitable areas. The IFD implies at least some use of a predictive orientation mechanisms, i.e. where individuals orientate towards areas in which the environment is predicted to be optimal, without following gradients in the near-field (Fernö et al. 1998). Our results suggest that a simple gradient search based on reactive as opposed to predictive orientation is best able to reproduce the mackerel distribution (Table 2, Fig. 5). This is supported by observations using sonar which indicate that NEAM swimming direction over summer is variable, suggesting reactions to food in the near field (Nottestad et al. 2016).

Our use of two feeding strategies with distinct assumptions about knowledge of the environment does not account for the possibility that NEAM may use a combination of both predictive and reactive orientation mechanisms. Nottestad et al. (2016) suggest that mackerel may use some directional cue to reach areas where feeding is predicted to be best, but react to local feeding opportunities along the way. An interesting possibility is that currents provide a directional cue (Nottestad et al. 2016). The North Atlantic Current enters the Nordic seas from the south. It branches into the Norwegian current, which flows Northwards into the Norwegian Sea, and the Irminger Current, which generally flows North and Westwards from the south of Iceland towards Greenland (Wanamaker et al. 2012; <https://oceancurrents.rsmas.miami.edu/atlantic/north-atlantic.html>). These currents are generally in line with the prevailing direction of the mackerel feeding migration, and could be used as a cue on which to base predictive orientation until they arrive at suitable feeding locations (i.e. areas of high prey density). In addition to the feeding migration, it has been suggested that *S.scombrus* use currents for navigation at other times of year. For example, in the Northwest Atlantic mackerel may use tidal streams to reach their spawning grounds

(Castonguay and Gilbert 1995). In future it may be possible to extend our IBM and include currents explicitly (see e.g. Scutt Phillips et al. (2018)).

Our GAS_{dd} model is in general agreement with the consensus that the summer distribution of Northeast Atlantic mackerel has shown a recent north and westward expansion (Berge et al. 2015, Nøttestad et al. 2015, Pacariz et al. 2016, Olafsdottir et al. 2018) (Fig. 6). It does, however, considerably under-predict the extent of the expansion in the western direction (Fig. 4). This could be explained by several factors. First, there is the possibility that NEAM use both reactive and predictive orientation (possibly based on currents) in order to navigate towards the most productive feeding grounds. In the IFD_{dd} search mechanism, which is based on predictive orientation, individuals inhabit areas west of Iceland in large densities (Fig. 8). Second, our IBM does not include any competing species. It would be difficult to extend our highly detailed approach from a single to multiple species (e.g. specifying bioenergetics and movement models for the full ontogeny of multiple species). Omission of competing species may be problematic, however, as it is not possible to account for the food limitation arising from interspecific competition which could force the mackerel into fringe areas. Indeed, there is high diet overlap between herring and mackerel in the Nordic seas (Bachiller et al. 2016), although species distribution modelling suggests that the two species can successfully cohabit (Nikolioudakis et al. 2018). Third, we use chlorophyll as a proxy for food availability. We use this data because it is available with greater coverage, spatial and temporal resolutions than that available for zooplankton. This does, however, leave our model vulnerable to the usual assumptions associated with extrapolating from primary to secondary production such as possible lag times between peaks of phyto- and zooplankton. In all, due to data and technical constraints, our results are limited to the effect of mackerel SSB, temperature and a proxy for food availability, and should be viewed as such.

Much of the variation in the summer distribution of mackerel appears to be explained by three main factors: a bottom-up effect of prey distribution; a density-dependent effect of mackerel stock size; and the effects of temperature (Pacariz et al. 2016, Nikolioudakis et al. 2018, Olafsdottir et al. 2018). We have incorporated these drivers into a mechanistic IBM which also explicitly accounts for movement behaviour. The IBM is able to match data on NEAM occurrence in the Nordic Seas over 2007 to 2015 reasonably well (Fig. 4). It is also able to produce a north and westward expansion (Fig. 6), although, interestingly, it fails to capture the extent of the observed expansion in the western direction. Despite performing reasonably well, it should be kept in mind that our IBM has only been validated using presence/ absence data. Moreover, the IESSNS survey in which this data was collected has variable spatial coverage between years, with greater coverage in more recent years (Nøttestad et al. 2015). The time-series is also relatively short at present as data are not available for the years 2008 and 2009 (Olafsdottir et al. 2018). As more data become available (in particular catch per unit effort) we plan to further validate our IBM.

The inclusion of environmentally-driven movement represents a significant improvement to the initial version of our IBM (Boyd et al. 2018). The model is now able to make predictions about both the spatial distribution of the mackerel stock and its population dynamics (though further validation, testing, and possibly development, is needed to ensure its predictive power). Other bioenergetics IBMs have been applied to the summer feeding distribution of Atlantic mackerel (Utne and Huse 2012, Heinänen et al. 2018). However, our model differs in that it is multi-generational and includes the full life cycle, i.e. what happens outside of the feeding period. This is important because distribution at one point in time is affected by both what has gone before and the need to close the life cycle (Payne et al. 2017). For example, in our model the production of a very strong year class could lead to an increase in SSB, which

would then have knock-on effects for the stock's distribution. It should be noted, however, that in our model movement outside of the feeding period is still to some extent hard-wired. In future the model could be extended to predict NEAM distribution at other times of year. For example, it may be possible to use the GAS model presented here to predict NEAM spawning distribution. The only difference would be that profitability would be some measure of habitat suitability for egg development as opposed to adult feeding opportunities. Data on egg distribution from the mackerel and horse mackerel egg survey (ICES 2013) could be used to validate the model. By modifying the movement models presented here and validating them with data on NEAM distribution outside of the feeding period, spatial distribution at other times of year could become a fully-emergent feature of the IBM.

Going forward we plan to use our IBM in a strategic capacity. For example, it could be used to project possible consequences of different environmental and management scenarios for NEAM. Forecasts of SST and chlorophyll, the environmental inputs needed for our model, are available under different anthropogenic emissions scenarios from several earth system models (ESMs). The outputs of ESMs are already being used as forcing for ecosystem and fisheries models as part of the fisheries and marine ecosystem model inter-comparison project (Lotze et al. 2018, Tittensor et al. 2018). As for management scenarios, our model is able to look at the effects of both spatial and temporal measures. Projections of how temporal management measures (e.g. catch limits) will affect fish stocks are already commonplace in tactical management (see ICES 2018 for NEAM catch scenarios). Predicting the likely effects of spatial management measures is, however, more difficult. Because our model is spatially-explicit, and predicts the geographical distribution of the mackerel population, it should be able to capture the local effects of spatial measures on the appropriate subset of the population. For these reasons we think that our model could be used to make predictions about how changes in environmental and spatial harvesting scenarios may affect the stock.

Acknowledgements

We would like to acknowledge NASA's Ocean Biology Processing Group for providing the satellite remote sensing data, and the National Oceanographic Data Centre for providing the bathymetric data. This work was supported by a NERC PhD studentship [grant number NE/L002566/1] with CASE sponsorship from CEFAS. We are grateful for helpful comments from three referees which have improved this paper.

Author contributions

RB led the writing of the manuscript and model development. All authors contributed to model development and gave critical comments on each draft of the manuscript. All authors gave permission for submission having seen the final draft.

References

- Bachiller, E., G. Skaret, L. Nøttestad, and A. Slotte. 2016. Feeding ecology of Northeast Atlantic mackerel, Norwegian spring-spawning herring and blue whiting in the Norwegian Sea. *PloS one* in press.
- Berge, J., K. Heggland, O. J. Lønne, F. Cottier, H. Hop, G. W. Gabrielsen, L. Nøttestad, and O. A. Misund. 2015. First records of Atlantic mackerel (*Scomber scombrus*) from the Svalbard Archipelago, Norway, with possible explanations for the extension of its distribution. *Arctic* 68:54–61.
- Boyd, R., S. Roy, R. Sibly, R. Thorpe, and K. Hyder. 2018. A general approach to incorporating spatial and temporal variation in individual-based models of fish

- populations with application to Atlantic mackerel. *Ecological Modelling* 382:9–17.
- Bruge, A., P. Alvarez, A. Fontán, U. Cotano, and G. Chust. 2016. Thermal Niche Tracking and Future Distribution of Atlantic Mackerel Spawning in Response to Ocean Warming. *Frontiers in Marine Science* 3:86.
- Brunel, T., C. J. G. van Damme, M. Samson, and M. Dickey-Collas. 2017. Quantifying the influence of geography and environment on the northeast Atlantic mackerel spawning distribution. *Fisheries Oceanography*:1–15.
- Cantor, S. B., C. C. Sun, G. Tortolero-Luna, R. Richards-Kortum, and M. Follen. 1999. A comparison of C/B ratios from studies using receiver operating characteristic curve analysis. *Journal of Clinical Epidemiology* 52:885–892.
- Castonguay, M., and D. Gilbert. 1995. Effects of tidal streams on migrating Atlantic mackerel, *Scomber scombrus* L.:941–954.
- Edwards, K. P., R. Barciela, and M. Butenschön. 2012. Validation of the NEMO-ERSEM operational ecosystem model for the North West European continental shelf. *Ocean Science* 8:983–1000.
- Evans, T. G., S. E. Diamond, and M. W. Kelly. 2015. Mechanistic species distribution modelling as a link between physiology and conservation. *Conservation Physiology* 3:1–16.
- Fernö, A., T. J. Pitcher, W. Melle, and L. Nøttestad. 1998. The challenge of the herring in the Norwegian Sea: making optimal collective spatial decisions. *Sarsia* 83:149–167.
- Formenti, P., G. Siour, M. Mallet, J. Sciare, G. Rea, L. Menut, S. Mailler, F. Meleux, S. Turquety, R. Briant, and B. Bessagnet. 2015. Ozone and aerosol tropospheric concentrations variability analyzed using the ADRIMED measurements and the WRF and CHIMERE models. *Atmospheric Chemistry and Physics* 15:6159–6182.
- Godø, O. R., V. Hjellvik, S. A. Iversen, A. Slotte, E. Tenningen, and T. Torkelsen. 2004. Behaviour of mackerel schools during summer feeding migration in the Norwegian Sea, as observed from fishing vessel sonars. *ICES Journal of Marine Science* 61:1093–1099.
- Grimm, V., U. Berger, F. Bastiansen, S. Eliassen, V. Ginot, J. Giske, J. Goss-Custard, T. Grand, S. K. Heinz, G. Huse, A. Huth, J. U. Jepsen, C. Jørgensen, W. M. Mooij, B. Müller, G. Pe'er, C. Piou, S. F. Railsback, A. M. Robbins, M. M. Robbins, E. Rossmannith, N. Rüger, E. Strand, S. Souissi, R. a. Stillman, R. Vabø, U. Visser, and D. L. DeAngelis. 2006. A standard protocol for describing individual-based and agent-based models. *Ecological Modelling* 198:115–126.
- He, P., and C. S. Wardle. 1988. Endurance at intermediate swimming speeds of Atlantic mackerel, *Scomber scombrus* L., herring, *Clupea harengus* L., and saithe, *Pollachius virens* L. *Journal of Fish Biology* 33:255–266.
- Heinänen, S., M. E. Chudzinska, J. Brandi Mortensen, T. Z. E. Teo, K. Rong Utne, L. Doksæter Sivle, and F. Thomsen. 2018. Integrated modelling of Atlantic mackerel distribution patterns and movements: A template for dynamic impact assessments. *Ecological Modelling* 387:118–133.
- Holloway, P., J. A. Miller, and S. Gillings. 2016. Incorporating movement in species distribution models: how do simulations of dispersal affect the accuracy and uncertainty of projections? *International Journal of Geographical Information Science* 30:2050–2074.
- Hughes, K. M., L. Dransfeld, and M. P. Johnson. 2014. Changes in the spatial distribution of

- 721 spawning activity by north-east Atlantic mackerel in warming seas: 1977–2010. *Marine*
722 *Biology* 161:2563–2576.
- 723 ICES. 2013. ICES Eggs and Larvae Dataset.
- 724 ICES. 2014a. Report of the Benchmark Workshop on Pelagic Stocks (WKPELA). *Ices Cm*
725 *Acom*: 43:7–125.
- 726 ICES. 2014b. Report of the Report of the Working Group on Widely Distributed Stocks
727 (WGWIDE) report 2014:37–192.
- 728 ICES. 2016. Report of the Working Group on Fish Distribution Shifts (WKFISHDISH), 22-
729 215 November, 2016, ICES HQ, Copenhagen, Denmark ICES CM 2016/ACOM: 55:1–
730 202.
- 731 ICES. 2017a. Mackerel (*Scomber scombrus*) in subareas 1–8 and 14, and in Division 9.a (the
732 Northeast Atlantic and adjacent waters):1–14.
- 733 ICES. 2017b. *Ices Wgwide Report* 2017:356–503.
- 734 ICES. 2018. Mackerel (*Scomber scombrus*) in subareas 1–8 and 14, and in Division 9.a (the
735 Northeast Atlantic and adjacent waters):1–14.
- 736 Jansen, T. 2014. Pseudocollapse and rebuilding of North Sea mackerel (*Scomber scombrus*).
737 *ICES Journal of Marine Science* 71:299–307.
- 738 Jansen, T., and F. Burns. 2015. Density dependent growth changes through juvenile and early
739 adult life of North East Atlantic Mackerel (*Scomber scombrus*). *Fisheries Research*
740 169:37–44.
- 741 Jansen, T., and H. Gislason. 2011. Temperature affects the timing of spawning and migration
742 of North Sea mackerel. *Continental Shelf Research* 31:64–72.
- 743 Jansen, T., and H. Gislason. 2013. Population Structure of Atlantic Mackerel (*Scomber*
744 *scombrus*). *PLoS ONE* 8.
- 745 Jansen, T., S. Post, T. Kristiansen, G. J. Skarsson, J. Boje, B. R. MacKenzie, M. Broberg, and
746 H. Siegstad. 2016. Ocean warming expands habitat of a rich natural resource and
747 benefits a national economy. *Ecological Applications* 26:2021–2032.
- 748 Liu, C., P. M. Berry, T. P. Dawson, and R. G. Pearson. 2005. Thresholds of Occurrence in the
749 Prediction of Species Distributions 28:385–393.
- 750 Lotze, H., D. Tittensor, A. Bryndum-Buchholz, T. Eddy, W. Cheung, E. Galbraith, M.
751 Barange, N. Barrier, D. Bianchi, J. Blanchard, L. Bopp, M. Bucher, C. Bulman, D.
752 Carozza, V. Christensen, M. Coll, J. Dunne, E. Fulton, S. Jennings, M. Jones, S.
753 Mackinson, O. Maury, S. Niiranen, R. Oliveros-Ramos, T. Roy, J. Fernandes, J.
754 Schewe, Y. Shin, T. Silva, J. Steenbeck, C. Stock, P. Verley, J. Volkholtz, and N.
755 Walker. 2018. Ensemble projections of global ocean animal biomass with climate
756 change. *In Review*:1–20.
- 757 McLane, A. J., C. Semeniuk, G. J. McDermid, and D. J. Marceau. 2011. The role of agent-
758 based models in wildlife ecology and management. *Ecological Modelling* 222:1544–
759 1556.
- 760 NASA OBPG. 2017a. Moderate-resolution Imaging Spectroradiometer (MODIS) Aqua
761 Chlorophyll-a OCI Algorithm Data; 2014 Reprocessing. NASA Goddard Space Flight
762 Center, Ocean Ecology Laboratory, Ocean Biology Processing Group., Greenbelt, MD,
763 USA.
- 764 NASA OBPG. 2017b. Moderate-resolution Imaging Spectroradiometer (MODIS) Aqua Sea

- Surface Temperature (daytime) Data; 2014 reprocessing. NASA Goddard Space Flight Center, Ocean Ecology Laboratory, Ocean Biology Processing Group., NASA OB.DAAC, Greenbelt, MD, USA.
- Nikolioudakis, N., H. J. Skaug, a H. Olafsdottir, T. Jansen, J. a Jacobsen, and K. Enberg. 2018. Drivers of the summer-distribution of Northeast Atlantic mackerel (*Scomber scombrus*) in the Nordic Seas from 2011 to 2017; a Bayesian hierarchical modelling approach. *ICES Journal of Marine Science*.
- Nottestad, L., J. Diaz, H. Pena, H. Sioland, G. Huse, and A. Ferno. 2016. Feeding strategy of mackerel in the Norwegian Sea relative to currents, temperature, and prey. *ICES Journal of Marine Science* 73:1127–1137.
- Nøttestad, L., S. P. Jo, J. A. Jacobsen, K. R. Utne, J. O. Guðmundur, Ø. Tangen, V. Anthonypillai, S. Aanes, J. H. Vølstad, M. Bernasconi, J. C. Holst, T. Jansen, A. Slotte, H. Debes, L. Smith, and S. Sveinbjo. 2015. Quantifying changes in abundance, biomass and spatial distribution of Northeast Atlantic mackerel in the Nordic seas from 2007 to 2014. *ICES Journal of Marine Science* 73:359–373.
- Olafsdottir, A. H., K. R. Utne, J. A. Jacobsen, T. Jansen, G. J. Óskarsson, L. Nøttestad, B. P. Elvarsson, C. Broms, and A. Slotte. 2018. Geographical expansion of Northeast Atlantic mackerel (*Scomber scombrus*) in Nordic Seas from 2007 - 2016 was primarily driven by stock size and constrained by low temperatures. *Deep-Sea Research Part II: Topical Studies in Oceanography*:0–1.
- Olafsdottir, A., A. Slotte, J. Arge Jacobsen, J. Gudmundur, G. Oskarssn, K. Utne, and L. Nottestad. 2016. Changes in weight-at-length and size-at-age of mature Northeast Atlantic mackerel from 1984:2013: effects of mackerel stock size and herring stock size 69:682–693.
- Pacariz, S. V., H. Hátún, J. A. Jacobsen, C. Johnson, S. Eliassen, and F. Rey. 2016. Nutrient-driven poleward expansion of the Northeast Atlantic mackerel (*Scomber scombrus*) stock: A new hypothesis. *Elementa: Science of the Anthropocene* 4:000105.
- Payne, M. R., A. J. Hobday, B. R. MacKenzie, D. Tommasi, D. P. Dempsey, S. M. M. Fässler, A. C. Haynie, R. Ji, G. Liu, P. D. Lynch, D. Matei, A. K. Miesner, K. E. Mills, K. O. Strand, and E. Villarino. 2017. Lessons from the First Generation of Marine Ecological Forecast Products. *Frontiers in Marine Science* 4.
- Pepin, P., J. A. Koslow, and S. Pearre. 1988. Laboratory study of foraging by Atlantic mackerel, *Scomber scombrus*, on natural zooplankton assemblages. *Can J Fish Aquat Sci* 45:879–887.
- Politikos, D., M. Huret, and P. Petitgas. 2015a. A coupled movement and bioenergetics model to explore the spawning migration of anchovy in the Bay of Biscay. *Ecological Modelling* 313:212–222.
- Politikos, D., S. Somarakis, K. Tsiaras, M. Giannoulaki, G. Petihakis, A. Machias, and G. Triantafyllou. 2015b. Simulating anchovy's full life cycle in the northern Aegean Sea (eastern Mediterranean): A coupled hydro-biogeochemical-IBM model. *Progress in Oceanography* 138:399–416.
- Robinson, N. M., W. A. Nelson, M. J. Costello, J. E. Sutherland, and C. J. Lundquist. 2017. A Systematic Review of Marine-Based Species Distribution Models (SDMs) with Recommendations for Best Practice. *Frontiers in Marine Science* 4:1–11.
- Sambily Jr, V. 1990. Interrelationships between swimming speed, caudal fin aspect ratio and body length of fishes.

- Scheffer, M., J. M. Baveco, D. L. Deangelis, K. a Rose, and E. H. Vannes. 1995. Super-Individuals A Simple Solution For Modeling Large Populations On An Individual Basis. *Ecological Modelling* 80:161–170.
- Scutt Phillips, J., A. Sen Gupta, I. Senina, E. van Sebille, M. Lange, P. Lehodey, J. Hampton, and S. Nicol. 2018. An individual-based model of skipjack tuna (*Katsuwonus pelamis*) movement in the tropical Pacific ocean. *Progress in Oceanography* 164:63–74.
- Sibly, R. M., V. Grimm, B. T. Martin, A. S. a Johnston, K. Kulakowska, C. J. Topping, P. Calow, J. Nabe-Nielsen, P. Thorbek, and D. L. Deangelis. 2013. Representing the acquisition and use of energy by individuals in agent-based models of animal populations. *Methods in Ecology and Evolution* 4:151–161.
- Teal, L. R., R. van Hal, T. van Kooten, P. Ruardij, and A. D. Rijnsdorp. 2012. Bio-energetics underpins the spatial response of North Sea plaice (*Pleuronectes platessa* L.) and sole (*Solea solea* L.) to climate change. *Global Change Biology* 18:3291–3305.
- Tittensor, D. P., T. D. Eddy, H. K. Lotze, E. D. Galbraith, W. Cheung, M. Barange, J. L. Blanchard, L. Bopp, A. Bryndum-Buchholz, M. Büchner, C. Bulman, D. A. Carozza, V. Christensen, M. Coll, J. P. Dunne, J. A. Fernandes, E. A. Fulton, A. J. Hobday, V. Huber, S. Jennings, M. Jones, P. Lehodey, J. S. Link, S. MacKinson, O. Maury, S. Niiranen, R. Oliveros-Ramos, T. Roy, J. Schewe, Y. J. Shin, T. Silva, C. A. Stock, J. Steenbeek, P. J. Underwood, J. Volkholz, J. R. Watson, and N. D. Walker. 2018. A protocol for the intercomparison of marine fishery and ecosystem models: Fish-MIP v1.0. *Geoscientific Model Development* 11:1421–1442.
- Trenkel, V. M., G. Huse, B. R. MacKenzie, P. Alvarez, H. Arrizabalaga, M. Castonguay, N. Goi, F. Gregoire, H. Hatun, T. Jansen, J. A. Jacobsen, P. Lehodey, M. Lutcavage, P. Mariani, G. D. Melvin, J. D. Neilson, L. Nottestad, G. J. Oskarsson, M. R. Payne, D. E. Richardson, I. Senina, and D. C. Speirs. 2014. Comparative ecology of widely distributed pelagic fish species in the North Atlantic: Implications for modelling climate and fisheries impacts. *Progress in Oceanography* 129:219–243.
- Tu, C. Y., Y. H. Tseng, T. S. Chiu, M. L. Shen, and C. H. Hsieh. 2012. Using coupled fish behavior-hydrodynamic model to investigate spawning migration of Japanese anchovy, *Engraulis japonicus*, from the East China Sea to Taiwan. *Fisheries Oceanography* 21:255–268.
- Uchmanski, J., and V. Grimm. 1996. Individual-based modelling in ecology: what makes the difference? 437–440.
- Uriarte, A., and P. Lucio. 2001. Migration of adult mackerel along the Atlantic European shelf edge from a tagging experiment in the south of the Bay of Biscay in 1994. *Fisheries Research* 50:129–139.
- Utne, K. R., S. S. Hjøllo, G. Huse, and M. Skogen. 2012. Estimating the consumption of *Calanus finmarchicus* by planktivorous fish in the Norwegian Sea using a fully coupled 3D model system. *Marine Biology Research* 8:527–547.
- Utne, K. R., and G. Huse. 2012. Estimating the horizontal and temporal overlap of pelagic fish distribution in the Norwegian Sea using individual-based modelling. *Marine Biology Research* 8:548–567.
- van der Vaart, E., M. a. Beaumont, A. S. a Johnston, and R. M. Sibly. 2015. Calibration and evaluation of individual-based models using Approximate Bayesian Computation. *Ecological Modelling* 312:182–190.
- van der Vaart, E., A. S. A. Johnston, and R. M. Sibly. 2016. Predicting how many animals

will be where: How to build, calibrate and evaluate individual-based models. *Ecological Modelling* 326:113–123.

Walsh, M., D. G. Reid, and W. R. Turrell. 1995. Understanding mackerel migration off Scotland: Tracking with echosounders and commercial data, and including environmental correlates and behaviour. *ICES Journal of Marine Science* 52:925–939.

Wanamaker, A. D., P. G. Butler, J. D. Scourse, J. Heinemeier, J. Eiríksson, K. L. Knudsen, and C. A. Richardson. 2012. Surface changes in the North Atlantic meridional overturning circulation during the last millennium. *Nature Communications* 3.

Watkins, K. S., and K. A. Rose. 2017. Simulating individual-based movement in dynamic environments. *Ecological Modelling* 356:59–72.